The Journal of Immunology

T Cell–Derived IL-17 Mediates Epithelial Changes in the Airway and Drives Pulmonary Neutrophilia

Laura K. Fogli, Mark S. Sundrud, Swati Goel, Sofia Bajwa, Kari Jensen, Emmanuel Derudder, Amy Sun, Maryaline Coffre, Catherine Uyttenhove, Jacques Van Snick, Marc Schmidt-Supprian, Anjana Rao, Gabriele Grunig, Joan Durbin, Stefano S. Casola, Klaus Rajewsky and Sergei B. Koralov

J Immunol 2013; 191:3100-3111; Prepublished online 21 August 2013;
doi: 10.4049/jimmunol.1301360
http://www.jimmunol.org/content/191/6/3100

The Journal of Immunology is published twice each month by
The American Association of Immunologists, Inc.,
1451 Rockville Pike, Suite 650, Rockville, MD 20852

Print ISSN: 0022-1767 Online ISSN: 1550-6606.

T Cell–Derived IL-17 Mediates Epithelial Changes in the Airway and Drives Pulmonary Neutrophilia

Laura K. Fogli,* Mark S. Sundrud,† Swati Goel,*,‡ Sofia Bajwa,* Kari Jensen,§ Emmanuel Derudder,¶ Amy Sun,* Maryaline Coffre,* Catherine Uyttenhove,‖ Jacques Van Snick,‖ Marc Schmidt-Supprian,# Anjana Rao, Gabriele Grunig,†† Joan Durbin,* Stefano S. Casola,‡‡ Klaus Rajewsky,§,1 and Sergei B. Koralov***

Th17 cells are a proinflammatory subset of effector T cells that have been implicated in the pathogenesis of asthma. Their production of the cytokine IL-17 is known to induce local recruitment of neutrophils, but the direct impact of IL-17 on the lung epithelium is poorly understood. In this study, we describe a novel mouse model of spontaneous IL-17–driven lung inflammation that exhibits many similarities to asthma in humans. We have found that STAT3 hyperactivity in T lymphocytes causes an expansion of Th17 cells, which home preferentially to the lungs. IL-17 secretion then leads to neutrophil infiltration and lung epithelial changes, in turn leading to a chronic inflammatory state with increased mucus production and decreased lung function. We used this model to investigate the effects of IL-17 activity on airway epithelium and identified CXCL5 and MIP-2 as important factors in neutrophil recruitment. The neutralization of IL-17 greatly reduces pulmonary neutrophilia, underscoring a key role for IL-17 in promoting chronic airway inflammation. These findings emphasize the role of IL-17 in mediating neutrophil-driven pulmonary inflammation and highlight a new mouse model that may be used for the development of novel therapies targeting Th17 cells in asthma and other chronic pulmonary diseases. ***The Journal of Immunology*****, 2013, 191: 3100–3111.**

Asthma, defined as a chronic condition characterized by lung inflammation and airway constriction, is loosely divided into the two main subsets of allergic and nonallergic asthma. Nonallergic asthma, also described as intrinsic or nonatopic, is a subtype of the disease that is often more severe than its allergy-triggered counterpart. Representing up to half of all asthma cases, nonatopic asthma is typically less responsive to steroid therapy and is characterized by neutrophilic infiltrates in the lungs (1). This neutrophilia is in contrast to the Th2 immune response and prominent eosinophilia typically seen in allergic asthma (2–4). The causal mechanisms of non-Th2 neutrophil-driven inflammation are not well understood, but Th17 cells have been suggested to play an important role.

Th17 cells are named for their production of IL-17A (IL-17), a proinflammatory cytokine that has been implicated in the initiation and progression of many chronic inflammatory diseases. IL-17 directly upregulates the expression of neutrophil-recruiting chemokines by fibroblasts in culture and lung tissue in vivo (5–7). Forced expression of IL-17 has been shown to induce neutrophil recruitment in rat airways, and mice deficient in IL-17 fail to develop lung inflammation upon immune challenge, demonstrating the potential importance of this cytokine to airway immunity (8, 9).

In humans, sputum from patients with steroid-resistant asthma contains elevated levels of IL-17 (10, 11), and higher IL-17 plasma levels in patients correlate with disease severity (12). Furthermore, elevated IL-17 levels have been shown in the sputum of patients with chronic obstructive pulmonary disease (COPD), a progressive inflammatory lung disease with clinical similarities to asthma (13). IL-17 has been suggested to play a role in the airway hyperresponsiveness seen in both of these conditions (14).

The development of Th17 cells requires STAT3, a member of the JAK/STAT family of signaling proteins. The initiation of the Th17 differentiation program occurs, in part, through IL-6 and IL-21 signaling and requires phosphorylation of STAT3 on tyrosine 705 (Y705) (15). In turn, activated STAT3 directs Th17 cell development through induction of the orphan nuclear receptor, RORγt, and also contributes directly to the transactivation of *Il17a* gene expression, via binding to conserved promoter elements (16). To study the role of IL-17–producing T cells in inflammatory diseases, we developed a mouse model in which a hyperactive STAT3 protein (STAT3C) is expressed selectively in T lymphocytes. In this study, we use this novel mouse model of chronic pulmonary inflammation to characterize the changes in the lung epithelium in-

*Department of Pathology, New York University School of Medicine, New York, NY 10016; †Department of Cancer Biology, The Scripps Research Institute, Jupiter, FL 33458; ‡Department of Hematology/Oncology, New York University School of Medicine, New York, NY 10016; §Immune Disease Institute, Boston, MA 02115; ¶Max Delbrück Center for Molecular Medicine, Berlin 13092, Germany; ‖Ludwig Institute, Brussels 1200, Belgium; #Max Delbrück Center for Biochemistry, Munich 82152, Germany; **La Jolla Institute for Allergy and Immunology, La Jolla, CA 92037 ††Department of Environmental Medicine, New York University School of Medicine, New York, NY 10016; and ‡‡The Institute of Molecular Oncology, Italian Foundation for Cancer Research, Milan 20139, Italy

[1]Current address: Max Delbrück Center for Molecular Medicine, Berlin, Germany.

Received for publication May 22, 2013. Accepted for publication July 21, 2013.

L.K.F. was supported by a New York University Vittorio Defendi Fellowship. M.S.S., K.R., and S.B.K. were supported by the GlaxoSmithKline/Immune Disease Institute alliance grant. A.R. was supported by National Institutes of Health Grants CA42471 and AI40127. G.G. was supported by National Institutes of Health Grant 1R01 HL095764-01. S.B.K. was supported by a New York University Whitehead Fellowship, a Feinberg Lymphoma Grant, and the Concern Foundation. L.K.F. and S.B.K. acknowledge the support of Cancer Center Support Grant for Shared Resources to New York University Cancer Institute, NCI 2P30CA016087-33.

Address correspondence and reprint requests to Dr. Sergei B. Koralov, Department of Pathology, New York University School of Medicine, 550 First Avenue, New York, NY 10016. E-mail address: sergei.koralov@nyumc.org

The online version of this article contains supplemental material.

Abbreviations used in this article: AB–PAS, Alcian blue and periodic acid-Schiff; BAL, bronchoalveolar lavage; COPD, chronic obstructive pulmonary disease; HPRT, hypoxanthine phosphoribosyltransferase; MMP, matrix metalloproteinase; qPCR, quantitative PCR; Treg, regulatory T cell.

www.jimmunol.org/cgi/doi/10.4049/jimmunol.1301360

duced by Th17 cells and to investigate how these changes lead to severe neutrophilia and structural changes characteristic of asthma and COPD.

Materials and Methods

Generation of the Stat3C allele and colony maintenance

Bruce4 C57BL/6 embryonic stem cells were transfected with a modified Rosa26 targeting vector containing a 5′ floxed stop/Neo cassette and FLAG-tagged *Stat3C* cDNA with an frt flanked IRES-eGFP downstream (Supplemental Fig. 1). Homologous recombination in embryonic stem cells was identified by Southern blot analysis for with a 5′ probe and Neo probe, and two clones were injected into blastocysts to generate chimeric animals that were then bred and maintained on a JAX C57BL/6 background. Mice were genotyped by PCR using the following primers for *Stat3C*^{stopfl}: forward, 5′-GATCATGGATTGTACCTGC-3′ and reverse, 5′-AGGTAGCACACTCCGAGG-3′, yielding a 600-bp product. Mice were maintained on a clean C57BL/6 background and housed in specific pathogen-free conditions at the Smilow barrier animal facility at NYU School of Medicine. Care of all animals was within institutional animal care committee guidelines, and all experiments were performed in accordance with approved protocols for the NYU Institutional Animal Care and Usage Committee. CD4Cre and R26YFP^{stopfl} mice were purchased from The Jackson Laboratory and maintained at the same NYU barrier facility for several generations. For most experiments (unless otherwise indicated), control animals with a floxed stop cassette but lacking CD4Cre, and Cre control littermates were used.

Flow cytometric analysis and sorting

To obtain a single-cell suspension for FACS analysis, lung samples were minced and dissociated in Liberase TL (Roche) for 35 min in a 37°C water bath. Liberase digestion was followed by mechanical disruption of the tissue through a 70-μm filter. Gut samples were prepared by isolating sections of small intestine, removing Peyer's patches, and digesting in Liberase TL (Roche) for 25 min at 37°C. Liberase was used at a concentration of 0.5 mg/ml in DMEM supplemented with 10% FBS. For analysis of bronchoalveolar lavage (BAL) fluid, tracheas of euthanized mice were cannulated with a 23-gauge blunt needle connected to a 1-ml syringe, and the lungs were flushed with 1 ml PBS. BAL samples were washed with FACS buffer (1% FBS and 1 mM EDTA in PBS) before surface staining. For intracellular cytokine staining, cells were first treated with a cell stimulation and protein transport inhibition mixture containing PMA, ionomycin, brefeldin A, and monensin (eBioscience) for 4 h. Cells were then surface stained, fixed in 2% paraformaldehyde, and permeabilized with 0.5% saponin, except for Foxp3 staining, which was performed using the Foxp3 Staining Buffer kit (eBioscience) according to the manufacturer's protocol. Fluorochrome-conjugated Abs with the following specificities were used, all from eBioscience except where noted: CD3, TCRβ, CD4, CD8 (Invitrogen), CD25, Gr1, Siglec-F (BD Biosciences), CCR3 (BD Biosciences), CD11b (BD Biosciences), F4/80, CCR3 (BD Biosciences), IL-17 (BioLegend), IL-22, IFN-γ, IL-4, Foxp3, and GFP (Invitrogen). Samples were acquired using a BD LSR II flow cytometer (BD Biosciences), and data were analyzed with FlowJo software (Tree Star). In all experiments, events were first gated using a gate that encompassed the live lymphocyte population (or a broader gate when analyzing granulocytes), followed by doublet exclusion using forward light scatter width versus forward light scatter height. Cells were then gated based on surface markers specific to the cell type of interest. Neutrophils were quantified based on staining with a Gr1 Ab (clone RB6-8C5), and their cell identity was confirmed with CD11b, CCR3, and F4/80 staining. Neutrophils were Gr1^{high}CD11b^{pos}F4/80^{neg}CCR3^{neg} with a high side scatter. Wild-type controls were mixed genotype; CD4Cre controls were included in analysis. Controls were age-matched, and littermates were used when possible. CD4$^+$ cells for quantitative PCR (qPCR) analysis were sorted using a MoFlo Legacy cell sorter (Beckman Coulter).

Quantitative real-time PCR analysis

Before preparation of RNA, lung samples were depleted of CD45$^+$ cells using anti-CD45 biotin Ab and anti-biotin microbeads (Miltenyi Biotec). Magnetic separation of cells was performed according to the manufacturer's protocol. CD45$^-$ cells were lysed, and RNA was prepared using an RNeasy mini kit (Qiagen). The samples were treated with DNase I on columns to eliminate any contamination with genomic DNA. The SuperScript VILO cDNA synthesis kit (Life Technologies) was used to prepare cDNA from RNA samples using random hexamers, and cDNA was then used as template for quantitative real-time PCR. qPCR was performed in a 20-μl reaction using SYBR Green master mix (Applied Biosystems) and the StepOnePlus Real-Time PCR system (Applied Biosystems). Hypoxanthine phosphoribosyltransferase (HPRT) was used as the endogenous control gene. Except where indicated, fold change values for each group relative to wild-type are shown. Relative fold change was calculated using the ΔΔ cycle-threshold method. Primer sequences used were as follows: CCL20 forward, 5′-GCTCACCTCTGCAGCCAGG-3′; CCL20 reverse, 5′-GTACGAGAGGCAACAGTCG-3′; CXCL5 forward, 5′-GCCGCTGGCATTTCTGTTG-3′; CXCL5 reverse, 5′-GCAAACACAACGCAGCTCC-3′; matrix metalloproteinase (MMP) 9 forward, 5′-CAGCCGACTTTTGTGGTC-3′; MMP9 reverse, 5′-GGGTGTAACCATAGCGGTAC-3′; GM-CSF forward, 5′-GCGCCTTGAACATGACAGC-3′; GM-CSF reverse, 5′-GGCTGTCTATGAAATCCGC-3′; IL-5 forward, 5′-GAGACCTTGACACAGCTGTC-3′; IL-5 reverse, 5′-GAGTAGGGACAGGAAGCCTC; IL-13 forward, 5′-GGTGCCAAGATCTGTGTCTC; IL-13 reverse, 5′-CACACTCCATACCATGCTGC; MIP-2 forward, 5′-CATCCAGAGCTTGAGTGTG-3′; MIP-2 reverse, 5′-GCTTCAGGGTCAAGGCAAAC-3′; CCR6 forward, 5′-CCATGACTGACGTCTACCTG-3′; CCR6 reverse, 5′-CAGTGCATCGCTGAAAACCC-3′; MMP2 forward, 5′-GTGATGGCT TCCTCTGGTG-3′; MMP2 reverse, 5′-CTTGCAGGGCTGTCCATCTG-3′; MMP7 forward, 5′-GGAGTGCCAGATGTTGCAG-3′; MMP7 reverse, 5′-GATCCACTACGATCCGAGG-3′; CD45 forward, 5′-GTCCCTACTTGCCTATGTC-3′; CD45 reverse, 5′-GCCGGGAGGTTTTCATTCC-3′; HPRT forward, 5′-GTCATGCCGACCCGCAGTC-3′; and HPRT reverse, 5′-GTCCTGTCCATAATCAGTCCATGAGGAATAAAC-3′.

Histopathology

Tissues were fixed in 10% formalin and stored in 70% EtOH before paraffin embedding. Lungs were inflated with formalin to open the air spaces before fixation. Tissues were cut into 5-μm sections and stained with H&E to visualize morphology or with Alcian blue and periodic acid-Schiff (AB–PAS) sequential staining to identify mucus-producing goblet cells and mucus plugs.

Measurement of respiratory mechanics

Mice were anesthetized by i.p. injection of a combination of xylazine (12 mg/kg) and sodium pentobarbital (70 mg/kg). Once absence of pedal reflex response was confirmed, mice were tracheotomized. A 19-guage thin-wall 0.5-inch metal cannula (Lab Express Management Company, Boston, MA) was inserted into the trachea and connected to a computer-controlled small animal ventilator (FlexiVent FX1; Scireq, Montreal, Canada). Mice were mechanically ventilated with 150 breaths/min at a tidal volume of 10 ml/kg. Ventilation was paused during pressure and volume perturbations to the lungs, which allow for the calculation of lung physiology parameters as previously described (17–19).

Tat-Cre transduction

For deletion of the stop cassette in vitro, R26Stat3C$^{stopfl/fl}$ and R26YFP$^{stopfl/fl}$ cells were washed three times to remove serum and then resuspended at 1×10^7 cells/ml in ADCF MAb medium (Thermo Scientific Hyclone) containing a final concentration of 50 μg/ml Tat-Cre. Cells were incubated for 45 min in a 37°C incubator, and the reaction was then terminated with the addition of serum-containing medium. Cells were washed and resuspended and allowed to rest for 4–6 h before being plated for T cell differentiation assays. Tat-Cre fusion protein has been previously described (20) and was obtained from Excellgen.

In vitro T cell differentiation assays

During all in vitro experiments, T cells were cultured in DMEM (Cellgro) supplemented with 10% FBS, nonessential amino acids (Cellgro), MEM essential vitamins (Life Technologies), 10 mM HEPES buffer (Cellgro), L-asparagine (36 μg/ml; Fisher Scientific), L-arginine–HCl (116 μg/ml; Fisher Scientific), folic acid (6 μg/ml; Fisher Scientific), penicillin-streptomycin (HyClone), L-glutamine (Life Technologies), and 50 μM 2-ME (Sigma-Aldrich).

For differentiation assays, CD4$^+$ T cells were magnetically separated from spleen and lymph nodes of 3–5-wk-old mice using MACS (Miltenyi Biotec) or Dynabeads (Invitrogen) negative selection kits, according to the manufacturer's instructions. In both cases, Ab cocktails were supplemented with anti-CD25 Ab to exclude regulatory T cells (Tregs) and activated T cells from the CD4$^+$ fraction. After cells were treated with Tat-Cre, they were resuspended at 5×10^6 cells/ml and plated under the various differentiation conditions shown. Cells were stimulated by plate-bound anti-CD3 (0.3 μg/ml) and anti-CD28 (0.5 μg/ml) Abs. The polarizing cytokines indicated were added at the following concentrations: human TGF-β1, 3 ng/ml; mouse IL-6, 30 ng/ml; mouse IL-12, 20 ng/ml; and mouse IL-4, 50 ng/ml. All were obtained from R&D Systems. The following neutralizing Abs were used: anti–IFN-γ (0.5 μg/ml), anti–IL-4

(0.5 μg/ml), and anti–IL-2 (1 μg/ml). rIL-2 (10 U/ml; BD Biosciences) was added to Th1, Th2, and Treg cultures after 48 h. Cells were cultured for a total of 4 to 5 d before intracellular cytokine staining and FACS analysis were performed. Data from multiple experiments were quantified by averaging the fold changes in differentiation upon Tat-Cre–mediated deletion of the stop cassette in R26YFP$^{stopfl/fl}$ and R26Stat3C$^{stopfl/fl}$ cells. This ratio was calculated by dividing the percentage of positively differentiated cells in the YFP$^+$ or GFP$^+$ population by the percentage of positively differentiated cells in the YFP$^-$ or GFP$^-$ population. The p values were calculated using the Mann–Whitney U test.

Treg suppression assays

Using the MACS Regulatory T Cell Isolation Kit (Miltenyi Biotec), CD4$^+$ T cells were magnetically isolated from spleen and lymph nodes of 3–5-wk-old mice and then further separated into CD25$^+$ and CD25$^-$ fractions. CD4$^-$ fraction was used for a feeder layer. Feeder cells were treated with 20 μg/ml mitomycin C to induce growth arrest and were then resuspended at a concentration of 5×10^5 cells/ml. CD4$^+$CD25$^-$ naive cells were labeled with CFSE and resuspended at 1×10^6 cells/ml. Tregs (CD4$^+$CD25$^+$ fraction) were plated at various concentrations, followed by CD4$^+$CD25$^-$ T cells, and then feeders. Soluble anti-CD3 Ab was added at a final concentration of 0.2 μg/ml to activate the T cells. Cultures were harvested 72 h later to assess for proliferation.

ELISA

IL-17 levels in the sera were measured using Meso Scale Discovery mouse IL-17 assay array kit (Meso Scale).

Neutralizing Ab treatment

Female mice pregnant with R26Stat3C$^{stopfl/fl}$ CD4Cre litters received 200 μg anti–IL-17 Ab (clone MM17F3) in PBS through i.p. injection. Once the pups were born, the females continued to be injected twice per week while nursing the litter. After the pups reached 10 d of age, they were subjected to injections of 200 μg twice per week for the duration of their lives. MM17F3 and its specificity for IL-17A have been previously described (21). Other litters were injected similarly with the isotype control IgG1 Ab (MOPC-21).

Statistical analysis

The nonparametric Mann–Whitney U test was used to determine statistical significance for flow cytometry, qPCR, ELISA, and FlexiVent data (Scireq). For survival data, the log-rank test was used. The p values <0.05 were considered to be statistically significant. Analysis was performed using GraphPad Prism (GraphPad).

Results

Generation of mice expressing hyperactive STAT3 in T cells

We generated mice with a targeted insertion of *Stat3C* into the ubiquitously expressed ROSA26 locus, as has been previously described (22) (Supplemental Fig. 1A, 1B). STAT3C differs from wild-type STAT3 only in two cysteine substitutions (A661C and N663C), resulting in disulfide linkage between two STAT3 monomers brought into proximity by Y705 phosphorylation and dimer

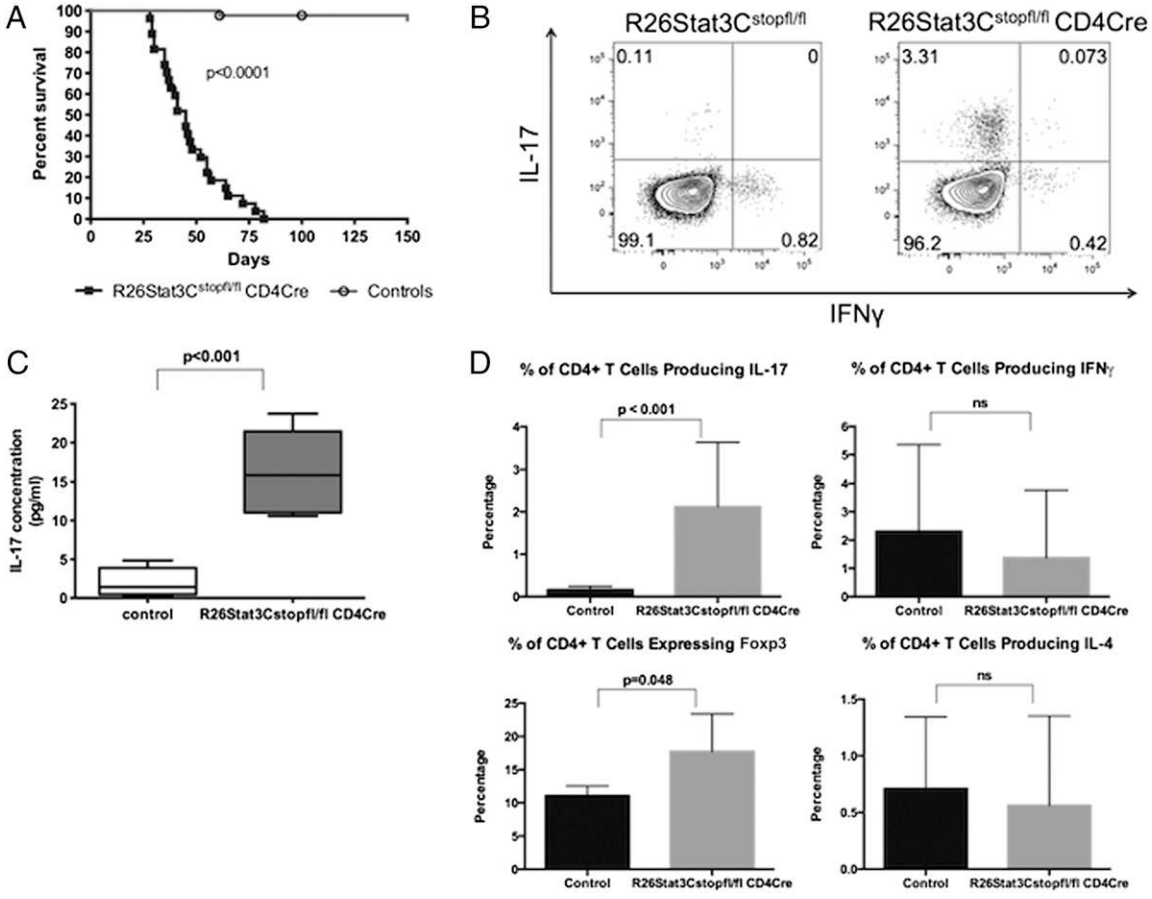

FIGURE 1. Expansion of Th17 cell population and dramatically shortened lifespan in R26Stat3C$^{stopfl/fl}$ CD4Cre mice. (**A**) Kaplan-Meier curve showing decreased survival in R26Stat3C$^{stopfl/fl}$ CD4Cre mice (filled squares) compared with controls (open circles). $n > 25$ for both groups; $p > 0.0001$. (**B**) Representative FACS analysis of CD4$^+$ T cells from peripheral lymph nodes of 8-wk-old R26Stat3C$^{stopfl/fl}$ CD4Cre mouse and control R26Stat3C$^{stopfl/fl}$ littermate. IL-17 and IFN-γ expression after 4 h PMA/ionomycin stimulation and brefeldin A treatment is shown. Events are gated on single CD4$^+$ lymphocytes. Data are representative of >10 experiments, with >15 mice/genotype. (**C**) IL-17 serum levels for R26Stat3C$^{stopfl/fl}$ CD4Cre mice and wild-type controls were analyzed by ELISA. $n \geq 5$ for both groups; $p < 0.001$. (**D**) Quantification of effector T cell populations in peripheral lymph nodes. For IL-17–producing, IFN-producing, and Foxp3$^+$ cell populations, data were collected from FACS analysis of at least eight independent experiments; $n \geq 7$ in R26Stat3C$^{stopfl/fl}$ CD4Cre group and $n \geq 5$ in control group. For IL-4–producing cells, data were collected from FACS analysis of three independent experiments; $n = 7$ in R26Stat3C$^{stopfl/fl}$ CD4Cre group and $n = 4$ in control group. Percentages were determined after gating on single CD4$^+$ cells within a lymphocyte gate.

stabilization (23, 24). CD4Cre-mediated deletion of an upstream stop cassette induces STAT3C expression in all T cells from the double-positive stage of thymic development. The targeted R26STAT3C^{stopfl} allele has an IRES-GFP sequence that leads to transcription of a bicistronic *Stat3C* EGFP mRNA, allowing for tracking of the cells in which the loxP-flanked stop cassette is deleted and STAT3C is expressed (Supplemental Fig. 1A). FACS analysis showed that nearly all peripheral T cells in the mutant mice expressed GFP and that T cell development in the thymus proceeded normally (Supplemental Fig. 1C, 1D).

STAT3C expression in naive T cells drives a bias toward the Th17 lineage

Expression of the hyperactive STAT3 protein in R26Stat3C$^{stopfl/fl}$ CD4Cre mice led to a drastically decreased average lifespan of 45 d (Fig. 1A). Analysis of lymph nodes and other secondary lymphoid organs showed a dramatic increase in IL-17 production by peripheral T cells, and IL-17 was detected at elevated levels in the serum of R26Stat3C$^{stopfl/fl}$ CD4Cre mice as well (Fig. 1B, 1C). Although murine Th17 cells also produce the closely related cytokine IL-17F, we focused our analysis on

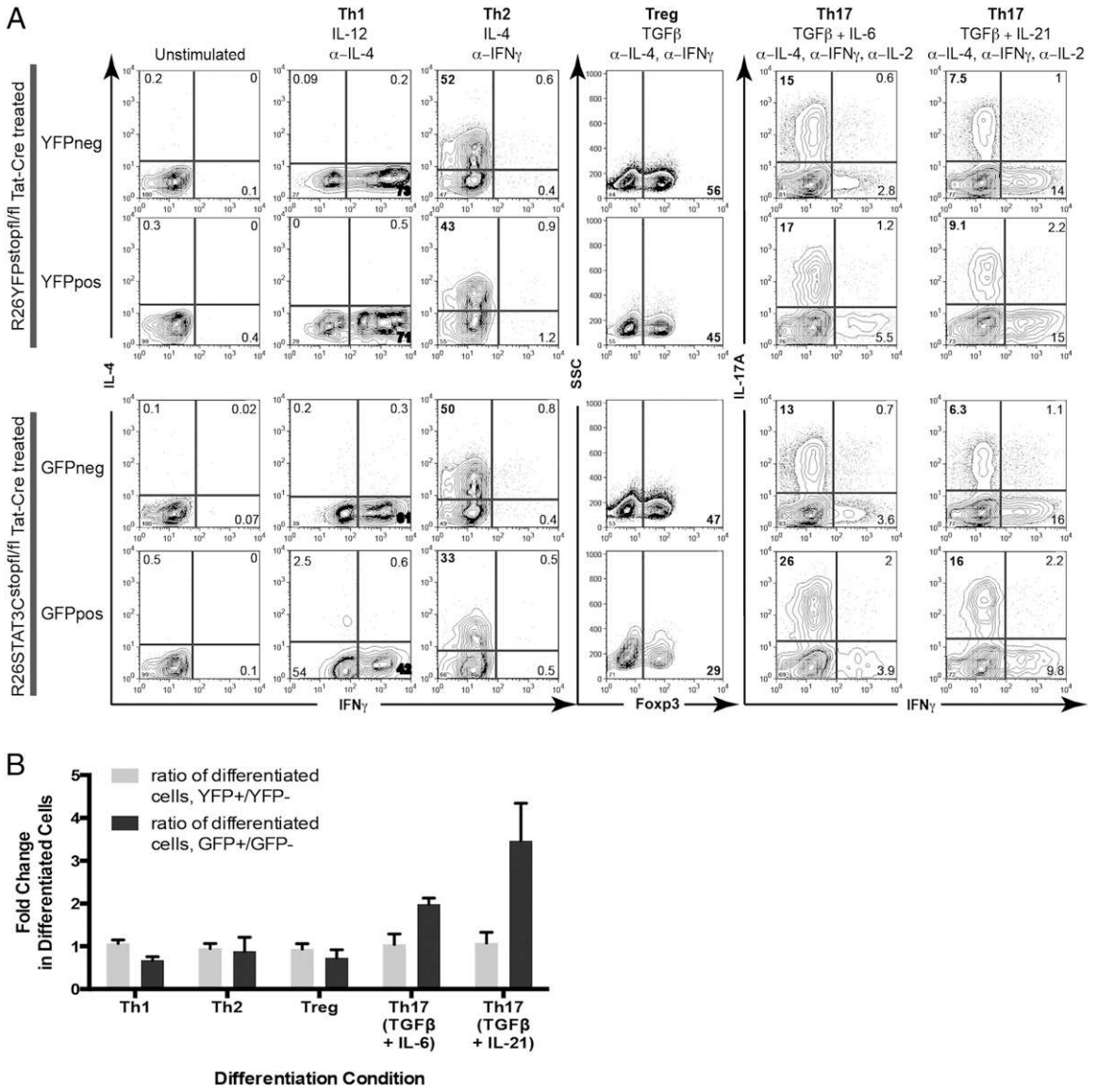

FIGURE 2. Impact of STAT3C expression on Th17 cell differentiation. (**A**) Representative FACS plots showing cytokine expression after in vitro T cell differentiation. CD4$^+$CD25$^-$ naive T cells were isolated from spleen and lymph nodes of 3–5-wk-old R26Stat3C$^{stopfl/fl}$ and R26YFP$^{stopfl/fl}$ mice. T cells were treated with transducible Cre protein (Tat-Cre) to induce the deletion of the stop cassette, then stimulated by plate-bound anti-CD3 and anti-CD28 Abs, and differentiated toward the Th1, Th2, Treg, and Th17 lineages with the indicated cytokines and neutralizing Abs. Cells were cultured for 4 d, and intracellular staining for cytokines was performed following 4 h PMA/ionomycin stimulation and brefeldin A treatment. Events shown are CD4$^+$ single lymphocytes gated based on GFP or YFP expression. Data are representative of more than three independent experiments. (**B**) Bar graph showing the fold change in differentiated CD4$^+$ T cells upon treatment with Tat-Cre in R26YFP$^{stopfl/fl}$ reporter cells or R26Stat3C$^{stopfl/fl}$ cells. Values shown are the average ratios of positively differentiated cells, calculated as the percentage in YFP$^+$ divided by the percentage in YFP$^-$ in control reporter cells or the percentage in GFP$^+$ divided by the percentage in GFP$^-$ in R26Stat3C$^{stopfl/fl}$ cells. Cells were plated under various differentiation conditions, including two conditions toward the Th17 lineage. Differentiation was determined by intracellular staining for cytokines in Th1, Th2, and Th17 or for Foxp3 in Tregs. Results are representative of three independent experiments, except for the Th17 (TGF-β + IL-6) condition, which is representative of seven independent experiments and has been shown to be statistically significant (for GFP$^+$/GFP$^-$; $p = 0.018$). Although a striking difference in the Th17 (TGF-β + IL-21) condition is evident, this difference does not reach statistical significance due to the small sample size.

IL-17A, as it is the most abundant IL-17 family member in mouse. FACS analysis did not show the expression of Th1 and Th2 cytokines IFN-γ and IL-4 to be significantly changed in mutant mice (Fig. 1D). Staining for the transcription factor Foxp3 indicated that Treg numbers were consistently higher in R26Stat3C$^{stopfl/fl}$ CD4Cre mice, indicating that any observed pathology was not a result of diminished Treg development (Fig. 1D).

To confirm that the hyperactivity of STAT3 in this model was directly causing an expansion of Th17 cells, we performed in vitro differentiation experiments using naive R26Stat3C$^{stopfl/fl}$ CD4$^+$ T cells, with R26YFP$^{stopfl/fl}$ CD4$^+$ cells as a control. We used Cre protein (Tat-Cre) transduction to delete the loxP-flanked stop cassette in vitro prior to differentiation of the naive T lymphocytes. GFP in STAT3C-expressing cells and YFP expression in T cells from R26YFP$^{stopfl/fl}$ mice allowed us to track cells in which

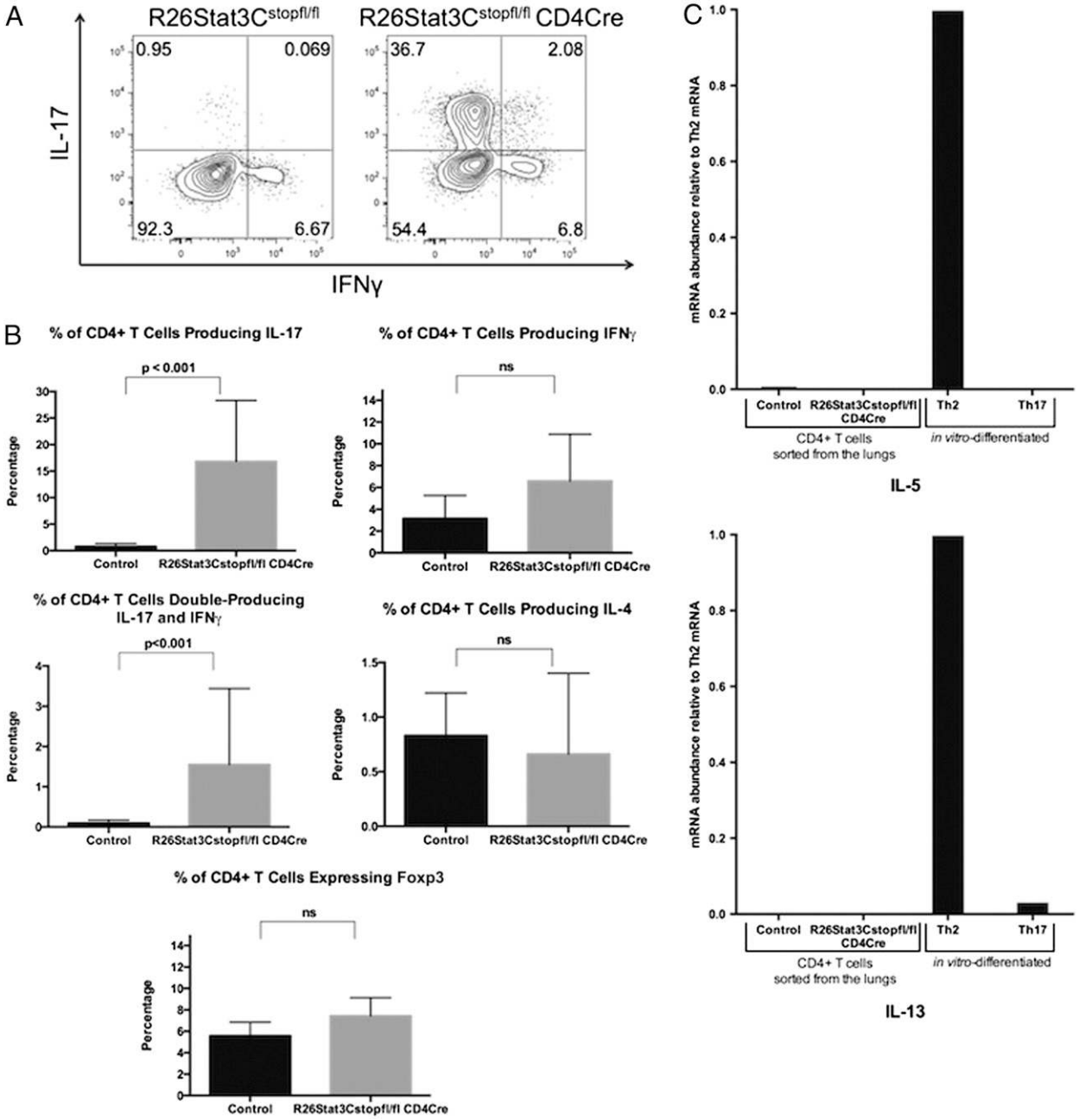

FIGURE 3. Increased IL-17 expression in the lungs of R26Stat3C$^{stopfl/fl}$ CD4Cre mice. (**A**) Representative FACS analysis of CD4$^+$ T cells in digested lungs of 8-wk-old R26Stat3C$^{stopfl/fl}$ CD4Cre mouse and control R26Stat3C$^{stopfl/fl}$ littermate. Intracellular staining for cytokines was performed following PMA/ionomycin stimulation as previously described. Events are gated on single CD4$^+$ lymphocytes. Data are representative of >10 experiments and >15 mice/genotype. (**B**) Quantification of T cell populations producing various cytokines in the lungs of 6–10-wk-old mice based on FACS analysis. Percentages of CD4$^+$ T cells rather than cell number were plotted, due to inconsistencies counting lymphocytes in epithelium-rich lung tissue. Percentages were determined after gating on single CD4$^+$ cells within a lymphocyte gate. Data were collected from ≥4 independent experiments. For IL-17–producing, IFN-producing, and IL-4–producing cell populations, $n \geq 9$ in both groups. For Tregs, $n = 8$ in R26Stat3C$^{stopfl/fl}$ CD4Cre group and $n = 5$ in control group. (**C**) qPCR analysis of IL-5 and IL-13 expression in CD4$^+$ T cells sorted from the lungs of R26Stat3C$^{stopfl/fl}$ CD4Cre and wild-type control mice. Single representative samples from the R26Stat3C$^{stopfl/fl}$ CD4Cre and control groups are shown, with in vitro–differentiated Th2 and Th17 cells included as controls. Values shown are relative to the Th2 control. Data are representative of two independent experiments.

deletion of the stop cassette occurred. Because our Tat-Cre treatment protocol results in the deletion of the stop cassette in 30–50% of the lymphocytes, cells in the same well that do not undergo Cre-mediated recombination serve as internal controls in these differentiation experiments. Under two different Th17-polarizing conditions, IL-17 expression was increased 2- to 3-fold in GFP$^+$ cells compared with GFP$^-$ control cells (Fig. 2A). This change was found to be statistically significant over multiple experiments in the Th17 condition using TGF-β and IL-6 (Fig. 2B). The level of IL-17 expression was unaffected by the Tat-Cre–mediated deletion of the stop cassette in YFP$^+$ reporter cells. Cytokine expression under the conditions for Th1, Th2, and Treg lineages was not significantly changed upon STAT3C expression (Fig. 2A, 2B). STAT3C-expressing cells that were cultured without Th17-polarizing cytokines did not begin producing IL-17, highlighting the requirement for an initial signaling event to induce active STAT3C dimers (data not shown). Thus, hyperactive STAT3 expression in naive T cells leads to increased differentiation toward the Th17 lineage upon activation.

Th17 cells in R26Stat3C$^{stopfl/fl}$ CD4Cre mice infiltrate the airways and cause severe neutrophilic lung inflammation

In addition to a Th17 bias in the peripheral lymphoid organs, mutant mice demonstrated striking Th17-driven inflammation, specifically in the lungs. FACS analysis on digested lungs indicated up to a 10-fold increase in Th17 cells, with an average of >15% of CD4$^+$ cells producing IL-17 in mutant mice (Fig. 3A, 3B). FACS analysis and histological studies of other tissues from mutant mice confirmed that the lung was the most affected organ. The CNS, pancreas, and liver displayed no signs of pathology or increase in Th17 cells, whereas the gut of R26Stat3C$^{stopfl/fl}$ CD4Cre mice showed increased number of Th17 lymphocytes, albeit less dramatic than that seen in the lung (data not shown).

FACS analysis of digested lung tissue from R26Stat3C$^{stopfl/fl}$ CD4Cre mice also revealed a modest increase in T cells producing IFN-γ, indicating a slight Th1 expansion (Fig. 3B). Interestingly, a fraction of IFN-γ–producing cells from the lungs of mutant mice coexpressed IL-17 (Fig. 3B), representing a polyfunctional subset of T cells that secrete both Th17 and Th1 cytokines and have been

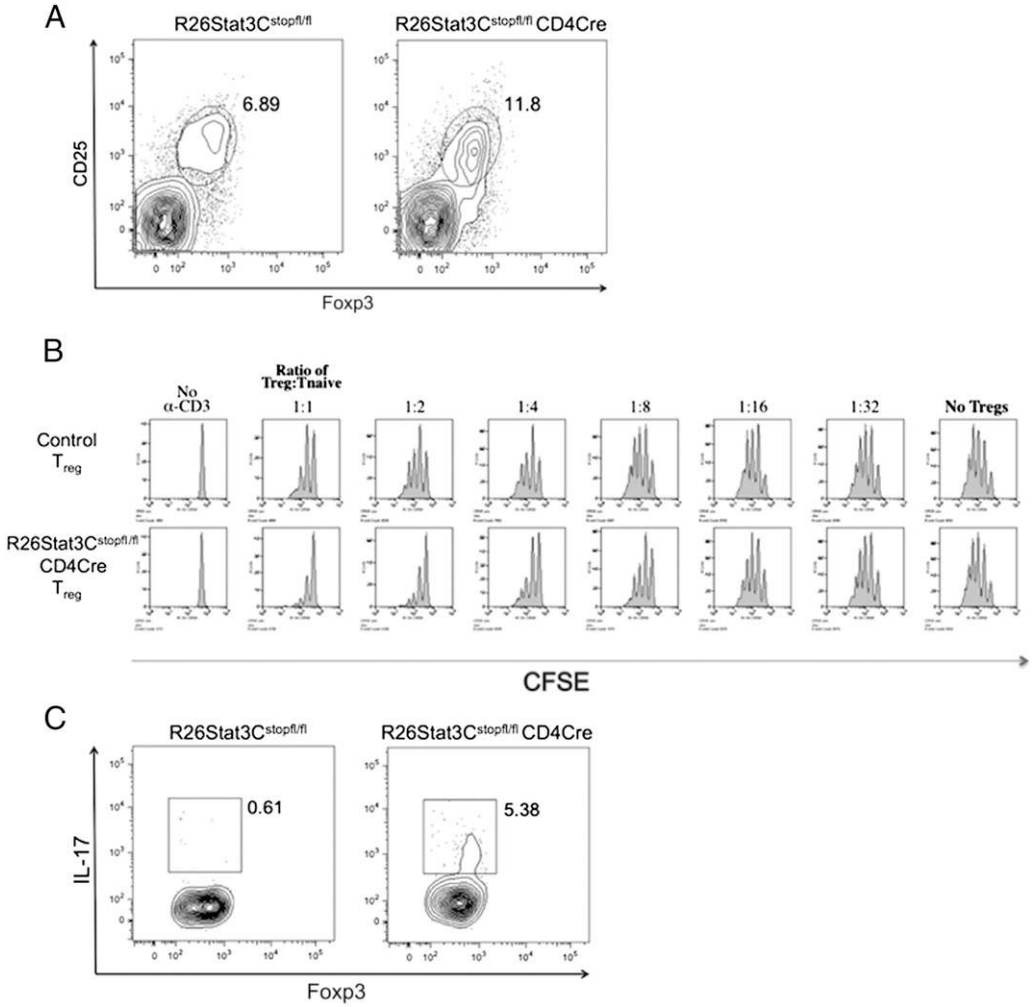

FIGURE 4. Functional Tregs present in the lungs of R26Stat3C$^{stopfl/fl}$ CD4Cre mice. (**A**) Representative FACS analysis showing CD25 and Foxp3 staining in digested lungs of 8-wk-old mice. Events are gated on single CD4$^+$ lymphocytes. FACS plots are representative of >10 independent experiments, with a total of at least 10 mice/genotype. (**B**) Histograms showing cell proliferation after in vitro Treg suppression assay. Wild-type naive CD4$^+$ T cells from 3- to 4-wk-old mice were plated with anti-CD3 Ab and varying concentrations of CD4$^+$CD25$^+$ Tregs from wild-type or R26Stat3C$^{stopfl/fl}$ CD4Cre mice. CFSE labeling was used to assess proliferation; cells were analyzed by FACS after 3 d in culture. Data are representative of three independent experiments. (**C**) IL-17 production by Tregs in the lymph nodes of R26Stat3C$^{stopfl/fl}$ CD4Cre mice. FACS analysis showing IL-17 expression in Foxp3$^+$ T cells from the lymph nodes of an 8-wk-old R26Stat3C$^{stopfl/fl}$ CD4Cre mouse and control littermate. Intracellular staining was performed following PMA/ionomycin stimulation as previously described. Events shown are gated on single CD4$^+$CD25$^+$Foxp3$^+$ lymphocytes. FACS plots are representative of three independent experiments.

described to be present specifically at sites of inflammation in both human and mouse (25). Th2 cells and the cytokines they produce are often implicated in eosinophil-driven lung inflammation; however, we did not observe an increase of Th2 cells in the lungs of STAT3C-expressing mice (Fig. 3B). This was confirmed through qPCR analysis of $CD4^+$ T cells for Th2 cytokines responsible for eosinophilia; IL-5 and IL-13 were not expressed by $CD4^+$ T cells sorted from the lungs of R26Stat3C$^{stopfl/fl}$ CD4Cre mice (Fig. 3C).

Consistent with results from lymph nodes, we observed slightly elevated levels of Tregs in the lungs of mutant mice, indicating that the generation of Tregs in the lungs of R26Stat3C$^{stopfl/fl}$ CD4Cre mice was not impaired (Figs. 3B, 4A). Furthermore, in vitro suppression assays revealed that STAT3C-expressing Tregs were functional and perhaps even slightly more efficient than wild-type Tregs at suppressing bystander T cell proliferation (Fig. 4B). Although a fraction of Tregs was secreting IL-17, the predominant source of T cell–derived IL-17 expression was $CD4^+Foxp3^-$ effector T cells (Fig. 4C).

Histopathology analysis of the lungs showed thickening of the airway epithelium, hypertrophy of the smooth muscle surrounding large and midsized airways, and pronounced perivascular and peribronchial/peribronchiolar inflammatory infiltrates (Fig. 5A). Furthermore, AB–PAS staining demonstrated metaplasia of mucus-secreting goblet cells and increased mucus production (Fig. 5B). Obstructive mucus plugs were observed within the bronchioles in >40% of examined sections from mutant mice, and a large number of muciphages, or mucus-containing macrophages, were present throughout the lungs of these animals (Fig. 5A, 5B). Although tissue sections showed a mixed inflammatory infiltrate consisting of lymphocytes, neutrophils, and a small percentage of eosinophils, FACS staining for Gr1 in digested lung tissue indicated that a large percentage of infiltrating leukocytes was neutrophils (Fig. 6A). We established that these $Gr1^{high}$ cells were neutrophils by confirming that they were $CD11b^{high}CCR3^{neg}F4/80^{neg}$ with a high side scatter (data not shown). Striking neutrophilia was also evident in BAL fluid (Fig. 6B). The marked increase in neutrophils in R26Stat3C$^{stopfl/fl}$ CD4Cre mice when compared with control littermates, together with no noticeable difference in eosinophil levels, represents an inflammatory profile characteristic of non-Th2 asthma. Lungs of control animals showed no pulmonary pathology.

Neutrophil attractants are upregulated by epithelial cells in the lungs of R26Stat3C$^{stopfl/fl}$ CD4Cre mice

As IL-17 is known to recruit neutrophils by acting directly on epithelial cells, we next performed qPCR analysis on lung parenchyma to identify target genes upregulated by IL-17 production. Total lungs were dissociated with a titrated mixture of purified collagenases to obtain a single-cell suspension. Tissue digestion was followed by depletion of $CD45^+$ cells through MACS to exclude leukocytes from our RNA analysis, and qPCR analysis of lung samples after MACS separation showed >95% depletion of CD45-expressing cells (data not shown). Our qPCR analysis revealed substantially elevated expression of CXCL5 in the lungs of R26Stat3C$^{stopfl/fl}$ CD4Cre mice compared with control lungs (Fig. 6C). CXCL5 (also called GCP-2) is a member of the CXC family of chemokines and a strong neutrophil attractant (26, 27). We also found a dramatic upregulation of MIP-2 in the lungs of mutant mice, observing an >7-fold increase compared with control mice (Fig. 6C). MIP-2, a functional mouse homolog of human IL-8, also promotes neutrophil migration and has been previously implicated in the airway only in an acutely induced model of lung inflammation (5, 28). The RNA levels of GM-CSF, another key factor in neutrophil recruitment that has been described to mediate airway inflammation (29), were analyzed in lung samples but unexpectedly were not found to be upregulated in mutant mice (Supplemental Fig. 2A). The upregulation of CXCL5 and MIP-2 indicates

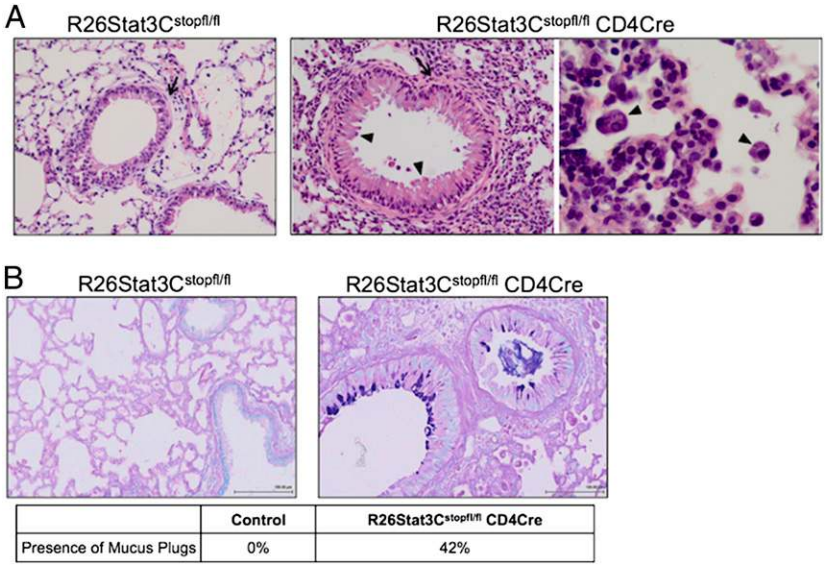

	Control	R26Stat3C$^{stopfl/fl}$ CD4Cre
Presence of Mucus Plugs	0%	42%

FIGURE 5. Severe inflammation and increased mucus production in the lungs of R26Stat3C$^{stopfl/fl}$ CD4Cre mice. (**A**) H&E staining of lungs from a wild-type control mouse (*left panel*) and R26Stat3C$^{stopfl/fl}$ CD4Cre mouse (*middle and right panels*). Wild-type control section shows an airway free of any signs of inflammation (original magnification ×200). Arrow indicates smooth muscle layer surrounding airway. *Middle panel* shows goblet cell metaplasia, alveolar inflammation, and smooth muscle hypertrophy causing thickening of the muscle layer in R26Stat3C$^{stopfl/fl}$ CD4Cre mouse (original magnification ×200). Arrow indicates smooth muscle layer surrounding airway, and arrowheads indicate the location of enlarged goblet cells lining the airway space. *Right panel* shows muciphages that contain large amounts of mucus in the alveolar space of the same R26Stat3C$^{stopfl/fl}$ CD4Cre mouse, indicated by arrowheads (original magnification ×600). (**B**) AB–PAS staining demonstrating a representative mucus plug obstructing an airway in an 8-wk-old R26Stat3C$^{stopfl/fl}$ CD4Cre mouse; original magnification ×200. The number of sections in which obstructive mucus plugs were observed was noted and is expressed as a percentage of examined sections in the table below. n = 8 for control group and n = 12 for R26Stat3C$^{stopfl/fl}$ CD4Cre group.

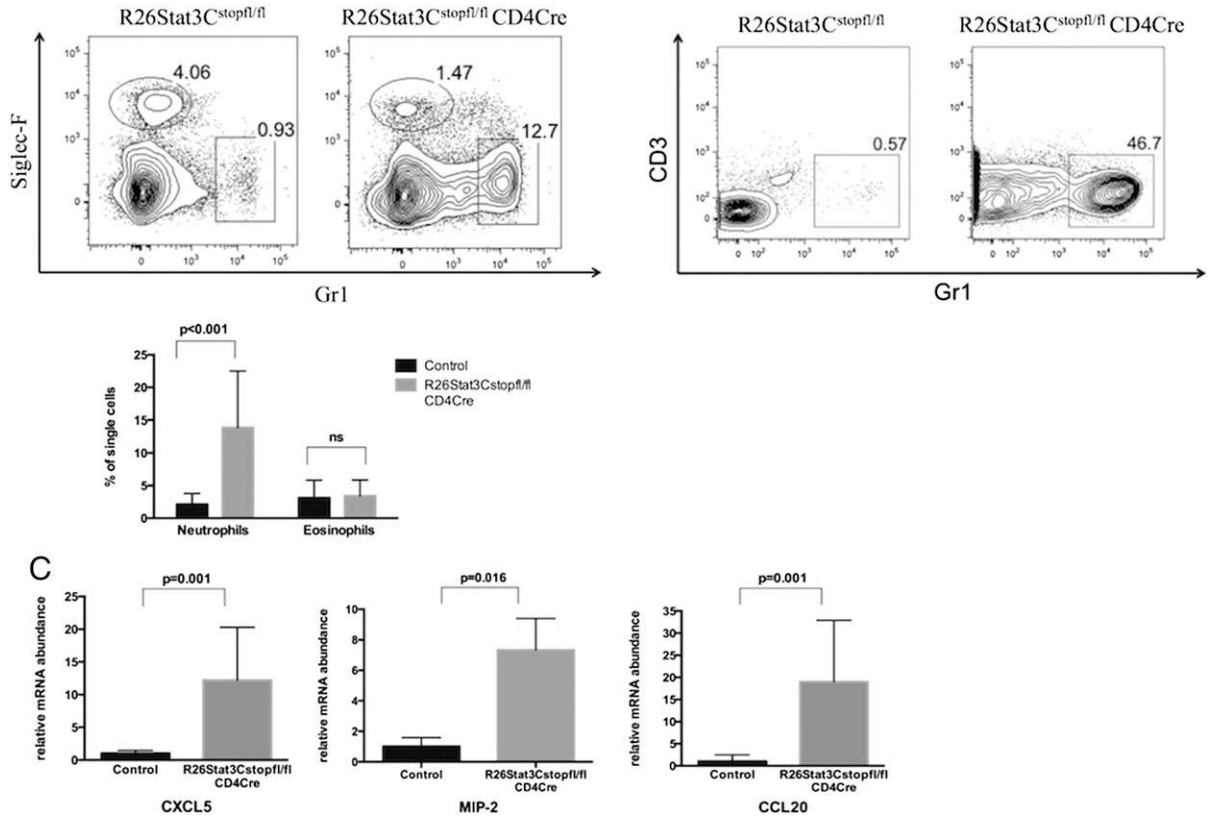

FIGURE 6. Neutrophilic infiltration and upregulation of chemokines by epithelial cells in the lungs. (**A**) Representative FACS plot and quantification of multiple experiments for neutrophils and eosinophil infiltration. FACS analysis shows Gr1 staining for neutrophils and Siglec-F staining for eosinophils in digested lungs. An 8-wk-old R26Stat3C$^{stopfl/fl}$ CD4Cre mouse and control R26Stat3C$^{stopfl/fl}$ littermate were used. Events shown are gated on single live cells. Gr1 staining is representative of >10 independent experiments, with a total of at least 10 mice/genotype. Siglec-F staining is representative of three independent experiments. Summary of eosinophil numbers is based on Siglec-F and/or CCR3 staining; $n \geq 5$ for both groups. (**B**) FACS analysis showing Gr1 staining in BAL fluid from 10-wk-old R26Stat3C$^{stopfl/fl}$ CD4Cre mouse and control littermate. Events are gated on single cells. Results are representative of three independent experiments. (**C**) qPCR analysis of CXCL5, MIP-2, and CCL20 in CD45$^-$ cells from lung, normalized to HPRT and relative to wild-type control. Successful depletion of CD45$^+$ cells from lung tissue was confirmed by qPCR. Data shown represent average values and SD from four independent experiments with each experiment containing one to two mice for each genotype. For CXCL5 and CCL20, $n = 7$ for R26Stat3C$^{stopfl/fl}$ CD4Cre group and $n = 5$ for control group. For MIP-2, $n = 5$ for R26Stat3C$^{stopfl/fl}$ CD4Cre group and $n = 4$ for control group.

a possible underlying mechanism for the dramatic Th17-driven neutrophilia seen in the lungs of R26Stat3C$^{stopfl/fl}$ CD4Cre animals and suggests that both MIP-2 and CXCL5 may be promising targets for the treatment of IL-17–induced pulmonary neutrophilia.

Lungs of R26Stat3C$^{stopfl/fl}$ CD4Cre mice also displayed a 15-fold increase in the expression of the chemokine CCL20, the ligand for CCR6, relative to control lungs (Fig. 6C). CCR6 is a marker of memory Th17 cells, and we have found it to be

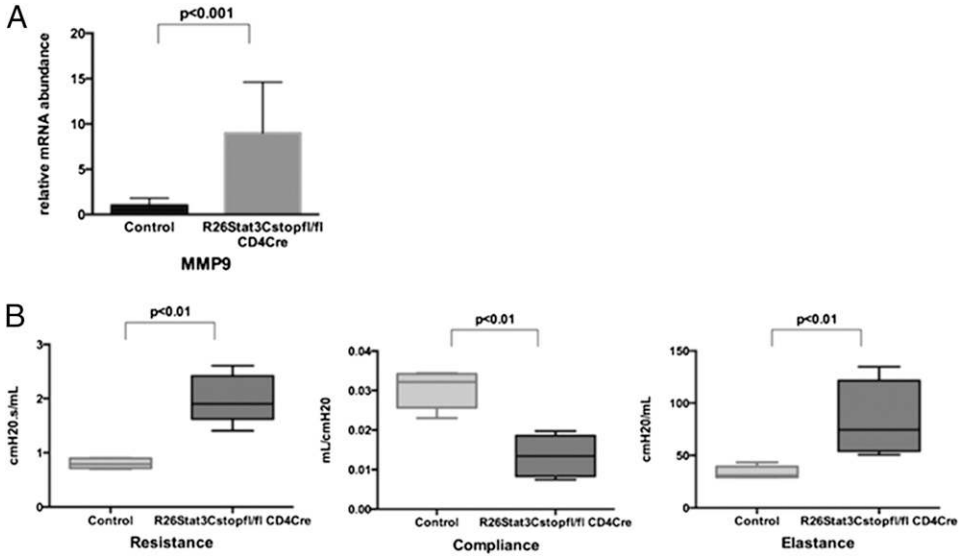

FIGURE 7. Increase in the remodeling factor MMP9 and impairment of normal lung function. (**A**) qPCR analysis of MMP9 in lung epithelial cells, normalized to HPRT and relative to wild-type control. RNA was prepared from digested lung samples after depletion of CD45$^+$ cells. Data was obtained from four independent experiments. $n = 7$ for R26Stat3C$^{stopfl/fl}$ CD4Cre group and $n = 5$ for control group. (**B**) Measurements of resistance, compliance, and elastance in the airway. Data are representative of three independent experiments; $n = 5$ for both groups.

expressed at elevated levels by $CD4^+$ cells present in the lungs of STAT3C mutant mice (30, 31) (Supplemental Fig. 3). The upregulation of CCL20 in the lungs suggests a positive-feedback loop in which IL-17 production recruits more CCR6-expressing Th17 cells to the tissue. We examined GM-CSF expression by $CD4^+$ T cells in STAT3C mutant mice, as Th17 cells have been described to produce GM-CSF in the context of inflammatory disease (32). However, no detectable GM-CSF expression was observed in sorted $CD4^+$ T cells from the lungs of control or R26Stat3C$^{stopfl/fl}$ CD4Cre mice, indicating that the neutrophilia and inflammatory changes in the lungs of mutant mice are due to effects of IL-17 on the epithelium, rather than direct recruitment of inflammatory cells by the Th17 cell population (Supplemental Fig. 2B).

Th17-induced inflammation leads to structural changes in the airways and impaired lung function

Expression of the remodeling factor MMP9 was highly upregulated by lung parenchyma isolated from Stat3C-expressing mice relative to control lungs, further highlighting the epithelial changes that result from increased levels of IL-17 expression in the lungs (Fig. 7A). The upregulation of MMP9, which degrades the extracellular matrix proteins collagen and laminin, is consistent with the airway remodeling observed in our histological analysis. Analysis of other MMPs, namely MMP2 and MMP7, did not reveal significant changes in expression between mutant and wild-type mice (data not shown).

To determine the effects of these structural changes on lung function, we measured parameters of respiratory mechanics in

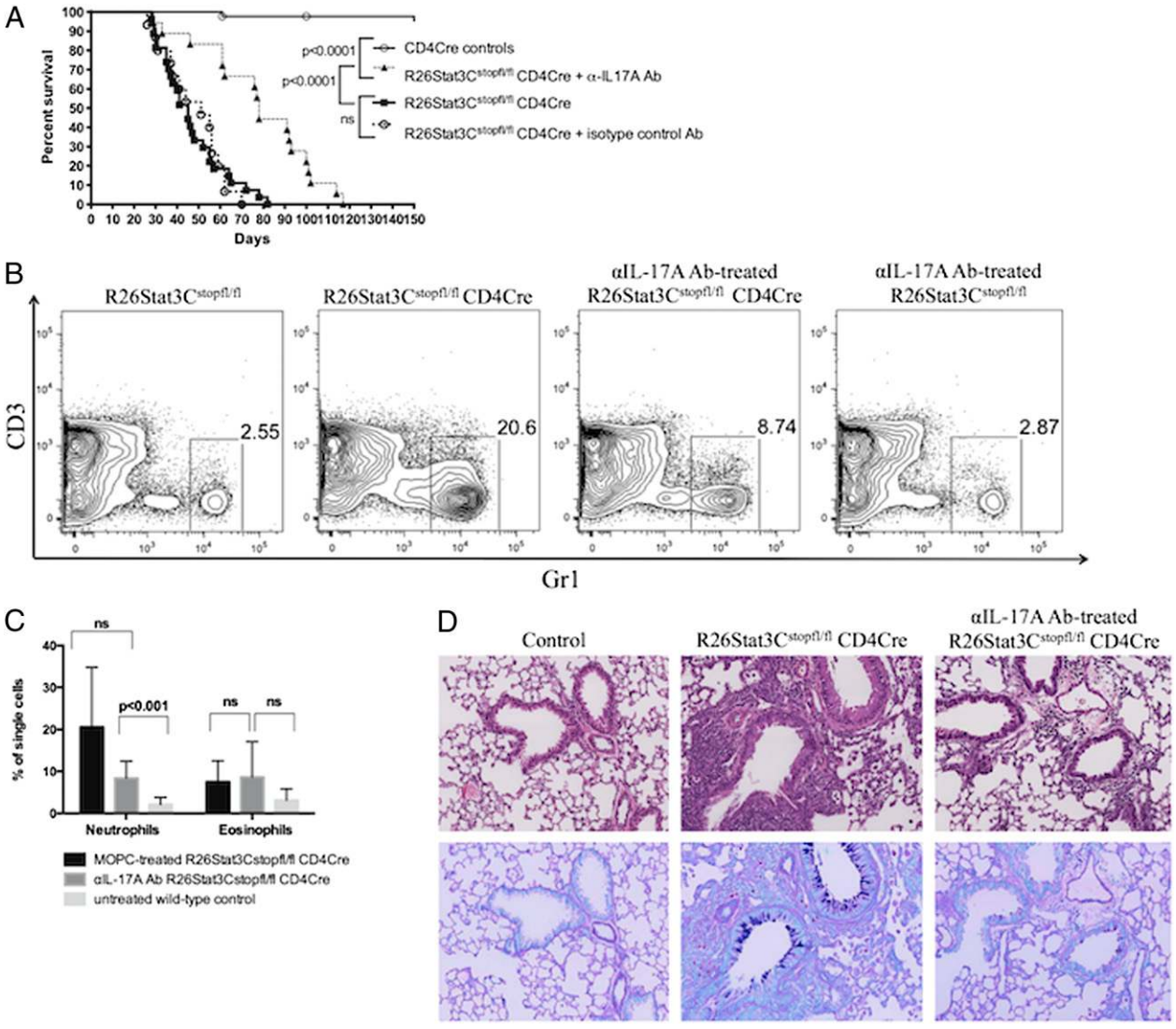

FIGURE 8. Increased survival and amelioration of lung inflammation in mice treated with IL-17–neutralizing Ab. (**A**) Kaplan-Meier curve showing survival of anti–IL-17 Ab–treated R26Stat3C$^{stopfl/fl}$ CD4Cre mice. As a control, survival of R26Stat3C$^{stopfl/fl}$ CD4Cre mice treated with an isotype control (MOPC-21) is also shown. $n > 15$ for all groups. $p < 0.0001$ for difference between untreated and anti–IL-17 Ab–treated R26Stat3C$^{stopfl/fl}$ CD4Cre mice, and $p < 0.0001$ for difference between anti–IL-17 Ab–treated R26Stat3C$^{stopfl/fl}$ CD4Cre and wild-type mice. There was no difference observed between MOPC-treated and untreated R26Stat3C$^{stopfl/fl}$ CD4Cre mice. (**B**) Representative FACS plot showing Gr1 staining in digested lungs of anti–IL-17 Ab–treated R26Stat3C$^{stopfl/fl}$ CD4Cre mice, compared with untreated R26Stat3C$^{stopfl/fl}$ CD4Cre animals. Age-matched treated and untreated R26Stat3C$^{stopfl/fl}$ controls are also shown. FACS analysis shown is from 8-wk-old mice. Data are representative of more than six independent experiments. (**C**) Quantification of neutrophils and eosinophils in the lungs, shown as percentages of total lung cells based on FACS analysis, in anti–IL-17 Ab–treated versus MOPC-treated R26Stat3C$^{stopfl/fl}$ CD4Cre mice. Four- to 10-wk-old mice were used. (**D**) Histological analysis of lungs from 6–12-wk-old mice: untreated R26Stat3C$^{stopfl/fl}$ CD4Cre, anti–IL-17 Ab–treated R26Stat3C$^{stopfl/fl}$ CD4Cre, and untreated control. *Top panel* shows H&E; *bottom panel* shows AB–PAS staining on the same section. Original magnification ×100. Histology is representative of more than four independent experiments.

R26Stat3C$^{stopfl/fl}$ CD4Cre mice using a forced-oscillation small animal ventilator. Airway resistance was consistently higher in mutant mice when compared with wild-type mice. We also observed a decrease in compliance and an increase in elastance in the mutant mice, together indicating a decreased elasticity of the lungs (Fig. 7B). These differences suggest severe lung function impairment and reflect the epithelial changes observed in non-Th2 asthma and other inflammatory lung diseases.

Expression of neutrophil chemoattractants and metalloproteinases by lung epithelial cells is IL-17 dependent

We next addressed the role of IL-17 in STAT3C-driven lung pathology by treating R26Stat3C$^{stopfl/fl}$ CD4Cre mice with an mAb against IL-17 (21). Mice treated with this neutralizing Ab from birth had a dramatically extended lifespan compared with untreated mice, and this difference was shown to be statistically significant (Fig. 8A). The improved lifespan was most likely due to a reduction in the amount of neutrophils infiltrating the lungs (Fig. 8B, 8C). Histopathological analysis showed that anti–IL-17 treatment ameliorated pulmonary inflammation, highlighted by fewer areas of infiltration, fewer mucus-producing goblet cells, and reduced frequency of mucus plugs (Fig. 8D and data not shown). The expression of CXCL5, MIP-2, and MMP9 in the lungs of R26Stat3C$^{stopfl/fl}$ CD4Cre mice was also dramatically reduced upon anti–IL-17 treatment, although the reduction in CXCL5 did not reach statistical significance (Fig. 9). The observed reduction in the expression of CXCL5, MIP-2, and MMP9 by the epithelial cells upon treatment with the neutralizing Ab supports the notion that these genes are downstream targets of IL-17 and underscores the role of T cell–derived IL-17A in chronic pulmonary inflammation, neutrophilia, and epithelial remodeling. We also observed a modest decrease in the expression of CXCL5 and MMP9 in anti–IL-17–treated wild-type controls as well, further supporting the notion that these genes are downstream targets of IL-17 (data not shown). The percentage of IL-17–expressing CD4$^+$ cells in the lungs and peripheral lymph nodes was not affected by the Ab treatment (Supplemental Fig. 4). Consistent with the migration of Th17 cells to the lungs of these mice even in the presence of neutralizing Ab, we did not observe a reduction of CCL20 upon treatment (Fig. 9). The striking improvement of the lung phenotype in the animals that received neutralizing anti–IL-17A Ab firmly establishes IL-17 as a key effector molecule secreted by Th17 cells that mediates neutrophil-driven lung inflammation.

Discussion

Signaling through STAT3 is essential for the differentiation of Th17 cells, a proinflammatory subset of T cells that has been implicated in airway inflammation. We have generated a mouse model in which hyperactive STAT3 is expressed selectively in T lymphocytes, leading to a pronounced Th17 bias and IL-17–mediated lung pathology.

Th17 cells predominantly produce IL-17, which has been shown to stimulate the production of inflammatory chemokines by neighboring epithelial cells and result in the recruitment of neutrophils (5, 7). We have shown that elevated Th17 cell numbers in the lungs of R26Stat3C$^{stopfl/fl}$ CD4Cre mice result in spontaneous neutrophilia, increased mucus production, and increased airway resistance characteristic of chronic inflammatory lung diseases, reaffirming a central role of these proinflammatory lymphocytes in pulmonary disease pathology. This Th17-driven inflammation occurs even in the presence of elevated numbers of functional Tregs in the lungs. It has been shown previously that Tregs are present in the lungs after allergen challenge, and although they are

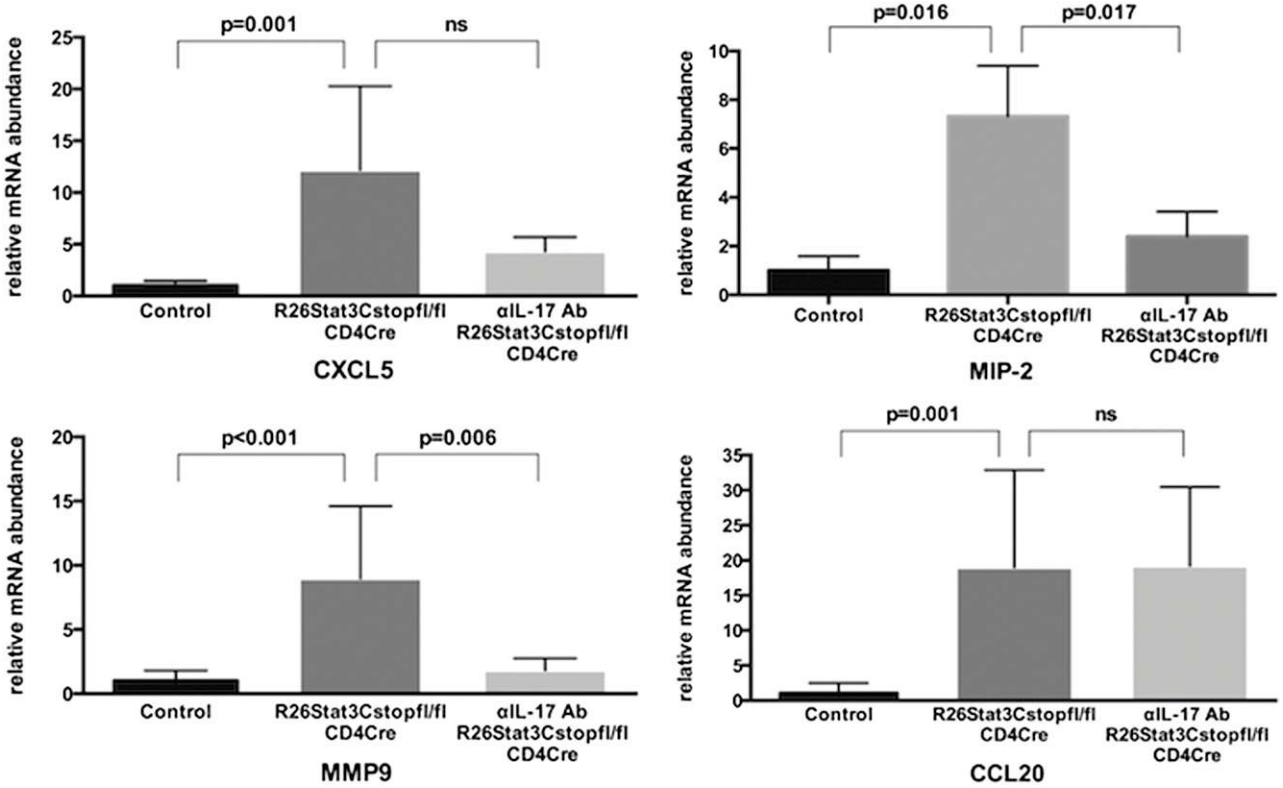

FIGURE 9. Downregulation of chemokines and remodeling factors in lungs of mice treated with IL-17–neutralizing Ab. qPCR analysis of CXCL5, MIP-2, MMP9, and CCL20, including R26Stat3C$^{stopfl/fl}$ CD4Cre treated with neutralizing Ab. Figure includes data from Figs. 7C and 8A, expanded with additional anti–IL-17 Ab–treated R26Stat3C$^{stopfl/fl}$ CD4Cre group. Four or more independent samples analyzed for all groups shown.

able to inhibit T cell proliferation, they are unable to suppress the production of Th2 cytokines (33). This seems to also be the case in this study, with Tregs unable to inhibit IL-17 production by the expanded population of Th17 cells that migrate to the airways. Although STAT3 has previously been implicated in altering stability of the natural Treg lineage by binding to the FoxP3 locus and thus preventing transactivation of FoxP3 by STAT5 (34–36), we did not observe any reduction in the level of FOXP3 within the Treg population. We also observed increased IL-17 production by $Foxp3^{+}CD25^{+}$ Tregs, underscoring the flexibility of this lineage and suggesting that in the presence of hyperactive STAT3, Tregs may not only be functional suppressor cells but may also produce the very cytokines of the inflammatory lineage they are attempting to control. Indeed, a population of $Foxp3^{+}$ cells that express IL-17 ex vivo have been described in humans, although the role of these cells in inflammation remains to be elucidated (37).

One of the striking features of the $R26Stat3C^{stopfl/fl}$ CD4Cre mice is that despite the fact that all T cells in these animals have an intrinsic propensity to differentiate toward the Th17 lineage, by far the greatest accumulation of these proinflammatory T cells that we observe is in the lungs. Further studies are necessary to elucidate the mechanisms that cause Th17 cells to home selectively to the lungs, but the upregulation of CCL20 by lung epithelial cells in $R26Stat3C^{stopfl/fl}$ CD4Cre mice suggests an interesting positive-feedback loop in which the presence of Th17 cells in the airways induces the recruitment of additional Th17 cells through CCL20/CCR6 signaling. It also may indicate an additional mechanism for recruitment of other inflammatory cells to the lungs, as CCL20 production by bronchial epithelial cells has been suggested to play a role in the migration of immune cells to the airway (38). RNA analysis of lung epithelial cells also indicated upregulation of the chemokines CXCL5 and MIP-2. CXCL5 is induced during acute lung inflammation, and its high expression has been shown to correlate with the exacerbation of asthma (39–41). The expression of CXCL5 is regulated in part by IL-17 signaling, as intratracheal administration of IL-17 in mice leads to upregulation of CXCL5 by alveolar type II cells in the lungs, and treatment of human alveolar type II cells in vitro has a similar effect (26). The functional human homolog of MIP-2, IL-8, is also found at high levels in severe asthma (10). In fact, expression of IL-8 correlates with increased expression of IL-17 in the sputum of asthmatics (42, 43). Our data suggest that CXCL5 and MIP-2 are both relevant targets of IL-17A in the context of spontaneous and chronic lung inflammation.

Surprisingly, our analysis of the lung epithelium did not show increased expression of GM-CSF, a well-described neutrophil recruitment factor. GM-CSF is often found to be upregulated in models of allergen-induced airway inflammation (44–46), and our observation may indicate that this cytokine is less relevant in instances of spontaneous lung inflammation. Additionally, we have shown that in the context of severe pulmonary inflammation, Th17 cells do not express GM-CSF. This is significant in light of the finding that the capacity of Th17 cells to produce GM-CSF is necessary for Th17-induced inflammation in the inflammatory disease model experimental autoimmune encephalomyelitis (32). Our results indicate that in chronic airway inflammation, it is the changes in the lung epithelium that occur in response to IL-17, as opposed to the production of other inflammatory cytokines by Th17 cells, that are responsible for the observed Th17-driven inflammation and neutrophil infiltration.

One of the distinguishing characteristics of asthma is the remodeling of the epithelium in the course of pulmonary inflammation, and our analysis of lung epithelial cells revealed an IL-17–dependent increase in MMP9. MMP9 degrades collagen and other structural proteins in the lungs, contributing to the airway remodeling often seen in asthma and COPD as the predominant MMP in these conditions (47–50). These changes in the lungs can affect respiratory function by increasing the rigidity of the airways, and indeed we saw a significant impact on lung function in $R26Stat3C^{stopfl/fl}$ CD4Cre mice. Respiratory measurements revealed increased airway resistance and elastance with decreased lung compliance, demonstrating a loss of normal lung structure and elasticity.

Although Th17 cells are described predominantly in nonatopic asthma, most asthma exacerbations are likely to have a non-Th2 component and some level of neutrophil infiltration, making this disease model and the identification of key roles for CXCL5, MIP-2, and MMP9 broadly applicable (51, 52). The goblet cell metaplasia and impairment in lung function observed in $R26Stat3C^{stopfl/fl}$ CD4Cre mice further demonstrate this model to be representative of inflammatory lung diseases seen in humans, namely asthma and COPD. $R26Stat3C^{stopfl/fl}$ CD4Cre mice can therefore serve as a novel disease model for the study of Th17- and neutrophil-driven chronic inflammatory lung disease, providing a new tool for the development of therapeutic strategies.

In summary, we have identified CXCL5, MIP-2, and MMP9 as targets of IL-17 activity in the context of chronic Th17-induced lung inflammation. The downregulation of these factors and marked improvement of lung disease upon neutralization of IL-17 indicates that IL-17 is, indeed, critical in driving the expression of inflammatory chemokines by airway epithelial cells and in the development of Th17-induced neutrophilic lung inflammation.

Acknowledgments

We thank the NYU Medical Center Histopathology Core and the NYU Medical Center Cytometry and Cell Sorting Core for expert assistance.

Disclosures

The authors have no financial conflicts of interest.

References

1. Bhakta, N. R., and P. G. Woodruff. 2011. Human asthma phenotypes: from the clinic, to cytokines, and back again. *Immunol. Rev.* 242: 220–232.
2. Douwes, J., P. Gibson, J. Pekkanen, and N. Pearce. 2002. Non-eosinophilic asthma: importance and possible mechanisms. *Thorax* 57: 643–648.
3. Gibson, P. G., J. L. Simpson, and N. Saltos. 2001. Heterogeneity of airway inflammation in persistent asthma : evidence of neutrophilic inflammation and increased sputum interleukin-8. *Chest* 119: 1329–1336.
4. Leung, D. Y., J. D. Spahn, and S. J. Szefler. 2002. Steroid-unresponsive asthma. *Semin. Respir. Crit. Care Med.* 23: 387–398.
5. Laan, M., Z. H. Cui, H. Hoshino, J. Lötvall, M. Sjöstrand, D. C. Gruenert, B. E. Skoogh, and A. Lindén. 1999. Neutrophil recruitment by human IL-17 via C-X-C chemokine release in the airways. *J. Immunol.* 162: 2347–2352.
6. McKinley, L., J. F. Alcorn, A. Peterson, R. B. Dupont, S. Kapadia, A. Logar, A. Henry, C. G. Irvin, J. D. Piganelli, A. Ray, and J. K. Kolls. 2008. TH17 cells mediate steroid-resistant airway inflammation and airway hyperresponsiveness in mice. *J. Immunol.* 181: 4089–4097.
7. Miyamoto, M., O. Prause, M. Sjöstrand, M. Laan, J. Lötvall, and A. Lindén. 2003. Endogenous IL-17 as a mediator of neutrophil recruitment caused by endotoxin exposure in mouse airways. *J. Immunol.* 170: 4665–4672.
8. Nakae, S., Y. Komiyama, A. Nambu, K. Sudo, M. Iwase, I. Homma, K. Sekikawa, M. Asano, and Y. Iwakura. 2002. Antigen-specific T cell sensitization is impaired in IL-17-deficient mice, causing suppression of allergic cellular and humoral responses. *Immunity* 17: 375–387.
9. Park, H., Z. Li, X. O. Yang, S. H. Chang, R. Nurieva, Y. H. Wang, Y. Wang, L. Hood, Z. Zhu, Q. Tian, and C. Dong. 2005. A distinct lineage of CD4 T cells regulates tissue inflammation by producing interleukin 17. *Nat. Immunol.* 6: 1133–1141.
10. Bullens, D. M., E. Truyen, L. Coteur, E. Dilissen, P. W. Hellings, L. J. Dupont, and J. L. Ceuppens. 2006. IL-17 mRNA in sputum of asthmatic patients: linking T cell driven inflammation and granulocytic influx? *Respir. Res.* 7: 135.
11. Hashimoto, T., K. Akiyama, N. Kobayashi, and A. Mori. 2005. Comparison of IL-17 production by helper T cells among atopic and nonatopic asthmatics and control subjects. *Int. Arch. Allergy Immunol.* 137(Suppl 1): 51–54.
12. Agache, I., C. Ciobanu, C. Agache, and M. Anghel. 2010. Increased serum IL-17 is an independent risk factor for severe asthma. *Respir. Med.* 104: 1131–1137.

13. Doe, C., M. Bafadhel, S. Siddiqui, D. Desai, V. Mistry, P. Rugman, M. McCormick, J. Woods, R. May, M. A. Sleeman, et al. 2010. Expression of the T helper 17-associated cytokines IL-17A and IL-17F in asthma and COPD. *Chest* 138: 1140–1147.
14. Barczyk, A., W. Pierzchala, and E. Sozañska. 2003. Interleukin-17 in sputum correlates with airway hyperresponsiveness to methacholine. *Respir. Med.* 97: 726–733.
15. Yang, X. O., A. D. Panopoulos, R. Nurieva, S. H. Chang, D. Wang, S. S. Watowich, and C. Dong. 2007. STAT3 regulates cytokine-mediated generation of inflammatory helper T cells. *J. Biol. Chem.* 282: 9358–9363.
16. Chen, Z., A. Laurence, Y. Kanno, M. Pacher-Zavisin, B. M. Zhu, C. Tato, A. Yoshimura, L. Hennighausen, and J. J. O'Shea. 2006. Selective regulatory function of Socs3 in the formation of IL-17-secreting T cells. *Proc. Natl. Acad. Sci. USA* 103: 8137–8142.
17. Wagers, S., L. Lundblad, H. T. Moriya, J. H. Bates, and C. G. Irvin. 2002. Nonlinearity of respiratory mechanics during bronchoconstriction in mice with airway inflammation. *J. Appl. Physiol.* 92: 1802–1807.
18. Schuessler, T. F., and J. H. Bates. 1995. A computer-controlled research ventilator for small animals: design and evaluation. *IEEE Trans. Biomed. Eng.* 42: 860–866.
19. Tomioka, S., J. H. Bates, and C. G. Irvin. 2002. Airway and tissue mechanics in a murine model of asthma: alveolar capsule vs. forced oscillations. *J. Appl. Physiol.* 93: 263–270.
20. Peitz, M., K. Pfannkuche, K. Rajewsky, and F. Edenhofer. 2002. Ability of the hydrophobic FGF and basic TAT peptides to promote cellular uptake of recombinant Cre recombinase: a tool for efficient genetic engineering of mammalian genomes. *Proc. Natl. Acad. Sci. USA* 99: 4489–4494.
21. Uyttenhove, C., and J. Van Snick. 2006. Development of an anti-IL-17A autovaccine that prevents experimental auto-immune encephalomyelitis. *Eur. J. Immunol.* 36: 2868–2874.
22. Ernst, M. B., C. M. Wunderlich, S. Hess, M. Paehler, A. Mesaros, S. B. Koralov, A. Kleinridders, A. Husch, H. Münzberg, B. Hampel, et al. 2009. Enhanced Stat3 activation in POMC neurons provokes negative feedback inhibition of leptin and insulin signaling in obesity. *J. Neurosci.* 29: 11582–11593.
23. Bromberg, J. F., M. H. Wrzeszczynska, G. Devgan, Y. Zhao, R. G. Pestell, C. Albanese, and J. E. Darnell, Jr. 1999. Stat3 as an oncogene. *Cell* 98: 295–303.
24. Li, L., and P. E. Shaw. 2006. Elevated activity of STAT3C due to higher DNA binding affinity of phosphotyrosine dimer rather than covalent dimer formation. *J. Biol. Chem.* 281: 33172–33181.
25. Boniface, K., W. M. Blumenschein, K. Brovont-Porth, M. J. McGeachy, B. Basham, B. Desai, R. Pierce, T. K. McClanahan, S. Sadekova, and R. de Waal Malefyt. 2010. Human Th17 cells comprise heterogeneous subsets including IFN-gamma-producing cells with distinct properties from the Th1 lineage. *J. Immunol.* 185: 679–687.
26. Liu, Y., J. Mei, L. Gonzales, G. Yang, N. Dai, P. Wang, P. Zhang, M. Favara, K. C. Malcolm, S. Guttentag, and G. S. Worthen. 2011. IL-17A and TNF-α exert synergistic effects on expression of CXCL5 by alveolar type II cells in vivo and in vitro. *J. Immunol.* 186: 3197–3205.
27. Ruddy, M. J., F. Shen, J. B. Smith, A. Sharma, and S. L. Gaffen. 2004. Interleukin-17 regulates expression of the CXC chemokine LIX/CXCL5 in osteoblasts: implications for inflammation and neutrophil recruitment. *J. Leukoc. Biol.* 76: 135–144.
28. Ano, S., Y. Morishima, Y. Ishii, K. Yoh, Y. Yageta, S. Ohtsuka, M. Matsuyama, M. Kawaguchi, S. Takahashi, and N. Hizawa. 2013. Transcription factors GATA-3 and RORγt are important for determining the phenotype of allergic airway inflammation in a murine model of asthma. *J. Immunol.* 190: 1056–1065.
29. Laan, M., O. Prause, M. Miyamoto, M. Sjöstrand, A. M. Hytönen, T. Kaneko, J. Lötvall, and A. Lindén. 2003. A role of GM-CSF in the accumulation of neutrophils in the airways caused by IL-17 and TNF-alpha. *Eur. Respir. J.* 21: 387–393.
30. Singh, S. P., H. H. Zhang, J. F. Foley, M. N. Hedrick, and J. M. Farber. 2008. Human T cells that are able to produce IL-17 express the chemokine receptor CCR6. *J. Immunol.* 180: 214–221.
31. Wan, Q., L. Kozhaya, A. ElHed, R. Ramesh, T. J. Carlson, I. M. Djuretic, M. S. Sundrud, and D. Unutmaz. 2011. Cytokine signals through PI-3 kinase pathway modulate Th17 cytokine production by CCR6+ human memory T cells. *J. Exp. Med.* 208: 1875–1887.
32. El-Behi, M., B. Ciric, H. Dai, Y. Yan, M. Cullimore, F. Safavi, G. X. Zhang, B. N. Dittel, and A. Rostami. 2011. The encephalitogenicity of T(H)17 cells is dependent on IL-1- and IL-23-induced production of the cytokine GM-CSF. *Nat. Immunol.* 12: 568–575.
33. Faustino, L., D. Mucida, A. C. Keller, J. Demengeot, K. Bortoluci, L. R. Sardinha, M. Carla Takenaka, A. S. Basso, A. M. Faria, and M. Russo. 2012. Regulatory T cells accumulate in the lung allergic inflammation and efficiently suppress T-cell proliferation but not Th2 cytokine production. *Clin. Dev. Immunol.* DOI: 10.1155/2012/721817.
34. Laurence, A., S. Amarnath, J. Mariotti, Y. C. Kim, J. Foley, M. Eckhaus, J. J. O'Shea, and D. H. Fowler. 2012. STAT3 transcription factor promotes instability of nTreg cells and limits generation of iTreg cells during acute murine graft-versus-host disease. *Immunity* 37: 209–222.
35. Yao, Z., Y. Kanno, M. Kerenyi, G. Stephens, L. Durant, W. T. Watford, A. Laurence, G. W. Robinson, E. M. Shevach, R. Moriggl, et al. 2007. Nonredundant roles for Stat5a/b in directly regulating Foxp3. *Blood* 109: 4368–4375.
36. Zorn, E., E. A. Nelson, M. Mohseni, F. Porcheray, H. Kim, D. Litsa, R. Bellucci, E. Raderschall, C. Canning, R. J. Soiffer, et al. 2006. IL-2 regulates FOXP3 expression in human CD4+CD25+ regulatory T cells through a STAT-dependent mechanism and induces the expansion of these cells in vivo. *Blood* 108: 1571–1579.
37. Ayyoub, M., F. Deknuydt, I. Raimbaud, C. Dousset, L. Leveque, G. Bioley, and D. Valmori. 2009. Human memory FOXP3+ Tregs secrete IL-17 ex vivo and constitutively express the T(H)17 lineage-specific transcription factor RORgamma t. *Proc. Natl. Acad. Sci. USA* 106: 8635–8640.
38. Reibman, J., Y. Hsu, L. C. Chen, B. Bleck, and T. Gordon. 2003. Airway epithelial cells release MIP-3alpha/CCL20 in response to cytokines and ambient particulate matter. *Am. J. Respir. Cell Mol. Biol.* 28: 648–654.
39. Jeyaseelan, S., H. W. Chu, S. K. Young, and G. S. Worthen. 2004. Transcriptional profiling of lipopolysaccharide-induced acute lung injury. *Infect. Immun.* 72: 7247–7256.
40. Jeyaseelan, S., R. Manzer, S. K. Young, M. Yamamoto, S. Akira, R. J. Mason, and G. S. Worthen. 2005. Induction of CXCL5 during inflammation in the rodent lung involves activation of alveolar epithelium. *Am. J. Respir. Cell Mol. Biol.* 32: 531–539.
41. Qiu, Y., J. Zhu, V. Bandi, K. K. Guntupalli, and P. K. Jeffery. 2007. Bronchial mucosal inflammation and upregulation of CXC chemoattractants and receptors in severe exacerbations of asthma. *Thorax* 62: 475–482.
42. Fujie, H., K. Niu, M. Ohba, Y. Tomioka, H. Kitazawa, K. Nagashima, T. Ohrui, and M. Numasaki. 2012. A distinct regulatory role of Th17 cytokines IL-17A and IL-17F in chemokine secretion from lung microvascular endothelial cells. *Inflammation* 35: 1119–1131.
43. Zrioual, S., M. L. Toh, A. Tournadre, Y. Zhou, M. A. Cazalis, A. Pachot, V. Miossec, and P. Miossec. 2008. IL-17RA and IL-17RC receptors are essential for IL-17A-induced ELR+ CXC chemokine expression in synoviocytes and are overexpressed in rheumatoid blood. *J. Immunol.* 180: 655–663.
44. Puljic, R., E. Benediktus, C. Plater-Zyberk, P. A. Baeuerle, S. Szelenyi, K. Brune, and A. Pahl. 2007. Lipopolysaccharide-induced lung inflammation is inhibited by neutralization of GM-CSF. *Eur. J. Pharmacol.* 557: 230–235.
45. Vlahos, R., S. Bozinovski, S. P. Chan, S. Ivanov, A. Lindén, J. A. Hamilton, and G. P. Anderson. 2010. Neutralizing granulocyte/macrophage colony-stimulating factor inhibits cigarette smoke-induced lung inflammation. *Am. J. Respir. Crit. Care Med.* 182: 34–40.
46. Cates, E. C., R. Fattouh, J. Wattie, M. D. Inman, S. Goncharova, A. J. Coyle, J. C. Gutierrez-Ramos, and M. Jordana. 2004. Intranasal exposure of mice to house dust mite elicits allergic airway inflammation via a GM-CSF-mediated mechanism. *J. Immunol.* 173: 6384–6392.
47. Hoshino, M., Y. Nakamura, J. Sim, J. Shimojo, and S. Isogai. 1998. Bronchial subepithelial fibrosis and expression of matrix metalloproteinase-9 in asthmatic airway inflammation. *J. Allergy Clin. Immunol.* 102: 783–788.
48. Lee, Y. C., H. B. Lee, Y. K. Rhee, and C. H. Song. 2001. The involvement of matrix metalloproteinase-9 in airway inflammation of patients with acute asthma. *Clin. Exp. Allergy* 31: 1623–1630.
49. Oshita, Y., T. Koga, T. Kamimura, K. Matsuo, T. Rikimaru, and H. Aizawa. 2003. Increased circulating 92 kDa matrix metalloproteinase (MMP-9) activity in exacerbations of asthma. *Thorax* 58: 757–760.
50. Belvisi, M. G., and K. M. Bottomley. 2003. The role of matrix metalloproteinases (MMPs) in the pathophysiology of chronic obstructive pulmonary disease (COPD): a therapeutic role for inhibitors of MMPs? *Inflamm. Res.* 52: 95–100.
51. Fahy, J. V., K. W. Kim, J. Liu, and H. A. Boushey. 1995. Prominent neutrophilic inflammation in sputum from subjects with asthma exacerbation. *J. Allergy Clin. Immunol.* 95: 843–852.
52. Lamblin, C., P. Gosset, I. Tillie-Leblond, F. Saulnier, C. H. Marquette, B. Wallaert, and A. B. Tonnel. 1998. Bronchial neutrophilia in patients with noninfectious status asthmaticus. *Am. J. Respir. Crit. Care Med.* 157: 394–402.

Corrections

Fogli, L. K., M. S. Sundrud, S. Goel, S. Bajwa, K. Jensen, E. Derudder, A. Sun, M. Coffre, C. Uyttenhove, J. Van Snick, M. Schmidt-Supprian, A. Rao, G. Grunig, J. Durbin, S. S. Casola, K. Rajewsky, and S. B. Koralov. 2013. T cell–derived IL-17 mediates epithelial changes in the airway and drives pulmonary neutrophilia. *J. Immunol*. 191: 3100–3111.

One of the senior author's name was published incorrectly as "Stefano S. Casola". The correct name is Stefano Casola.

www.jimmunol.org/cgi/doi/10.4049/jimmunol.1390058